Paper No. 368. (quote when citing this article)
Eleventh World Conference on Earthquake Engineering
ISBN: 0 08 042822 3

CENTRIFUGE MODEL TESTS OF PILE FOUNDATION IN LIQUEFIABLE SAND DEPOSITS

ATSUNOBU FUKUOKA, NAOHITO ADACHI
Kajima Technical Research Institute, Kajima Corporation
19-1, Tobitakyu 2-chome, Chofu-shi, Tokyo 182, JAPAN

YUJI MIYAMOTO and YUJI SAKO
Kobori Research Complex, Kajima Corporation
KI Building, 6-5-30, Akasaka, Minato-ku, Tokyo 107, JAPAN

ABSTRACT

The responses of a pile foundation in liquefiable sand deposits are significantly affected by soil nonlinearity and excess pore water pressure generation during strong earthquakes. It is important to develop an understanding of the responses of pile foundations and pile bending moments in liquefied soil. In this study, shaking table tests for a four-pile-foundation model in saturated fine sand were carried out under a centrifuge acceleration of 45g. Correlation analyses using a beam-interaction spring model were conducted to investigate the responses of the pile foundation and the bending moment of the pile induced by the inertial and kinematic interactions. The response characteristics of pile foundation changed depending on the input level of acceleration and the weight of the structure. With increase in input acceleration, the effect of the inertial force of the structure on the pile bending moment decreased at the pile head but reached a deeper part of the pile. The pile bending moments caused by the relative displacement of the soil became larger. The numerical model of the soil-pile foundation system employed in this study followed well the pile foundation responses in a liquefied sand deposit.

KEYWORDS

Liquefaction; Pile Foundation; Centrifuge Model Test; Earthquake Response; Pile Bending Moment; Effective Stress Analysis; Lumped Mass Model; Nonlinear Soil Spring

1 INTRODUCTION

Many buildings are constructed on pile foundations embedded in loose sand that may liquefy during strong earthquakes. It has been pointed out that pile foundation responses in liquefied soil change remarkably due to large soil displacement and excess pore water pressure. To evaluate pile foundation responses in liquefied soil accurately, nonlinear soil-pile foundation interaction as well as excess pore water pressure generation must be taken into account. Model tests and earthquake observations are also needed to confirm the analytical procedures. Since very few records observed during strong earthquakes are available, dynamic centrifuge tests which can produce the same condition on overburden pressures in the field is effective in studying the behavior of pile foundations in liquefiable soil deposits. This paper describes centrifuge tests carried out on a four-pile-foundation model in saturated fine sand. Correlation analyses were also performed using a practical numerical model proposed by Miyamoto *et al.*(1992). This paper investigates the responses of the soil and the pile foundation and discusses the pile bending moments induced by the inertial force of the structure and the kinematic deformation of the soil deposit.

2 TEST CONDITIONS

The geotechnical centrifuge at Kajima Technical Research Institute was employed. It has an effective radius of 2.7m and is equipped with an electro-hydraulic shaker. The tests were performed under a centrifugal acceleration of 45g. Fig. 1 shows the centrifuge test model with the positions of measuring instruments. The dimensions in

Fig. 1 are indicated in prototype scale, which is 45 times of the model scale. The laminar box has the inside dimensions of length L=50cm, width W=20cm and height H=48cm. The pile foundation model was set up in saturated Toyoura sand of about 60 % relative density. The sand deposit was made by dry pluviation in the laminar box. The deposited sand was then vacuumed and saturated by introducing pore fluid from the base. Silicon oil, which has a viscosity 50 times greater than water, was employed for the pore fluid. The pile foundation model consisted of a four-pile group and a rigid pile cap which represented the inertial force of the superstructure. The model pile represented a prototype tubular-steel pile of diameter 0.7m, wall thickness 14mm and length 20.7m, with a pile spacing of 5.3 diameters. The pile cap was rigidly connected to the piles, which were processed so as to behave like pins at their tips. The NS component of El Centro 1940 was used for the input wave.

The test cases are summarized in Fig. 2 for the prototype unit. Two models with identical piles but with superstructures of different weights were employed to compare the effects of the different inertial forces. Two tests with different input accelerations were conducted for each model.

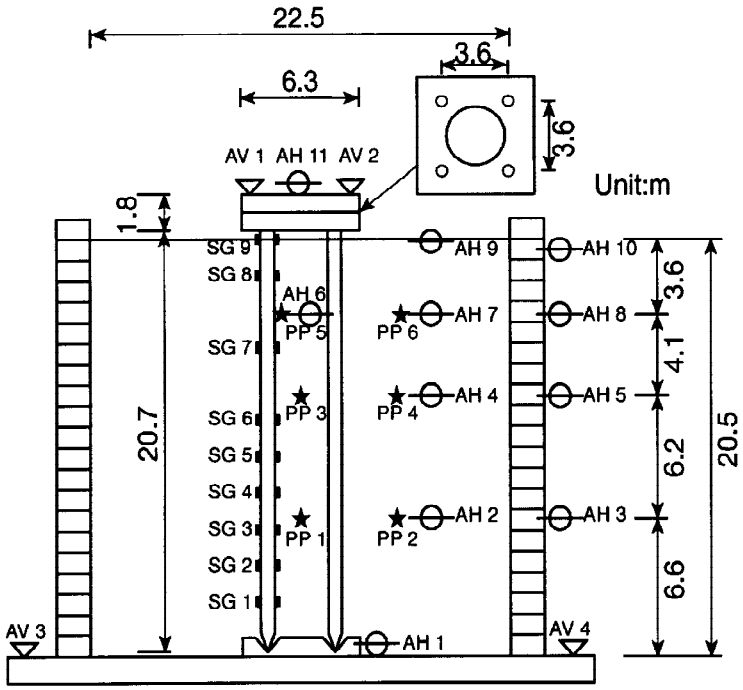

Fig. 1 Centrifuge test model (indicated in prototype scale) and measuring instruments

Test case	Structure weight (tf)	Input max. acc. (Gal)	Model
A 1	300	5.9	
A 2		114.3	
B 1	80	3.1	
B 2		110.4	

Fig. 2 Test cases of soil-pile foundation system

3 NUMERICAL MODEL

Correlation analyses were carried out using a beam-interaction spring model, as shown in Fig. 3. The pile foundation was modeled as lumped masses connected with bending-shear elements. Analyses for seismic response of the soil-pile foundation system were conducted at the following two stages. Firstly, the soil responses were calculated by the nonlinear effective stress analysis, the computer code DESRA proposed by Finn *et al.*(1977). Then, the obtained displacement and excess pore water pressure time histories at each depth were applied through the corresponding nonlinear lateral interaction soil springs. The linear rotational spring related to the axial stiffness of the piles was also incorporated into the pile head.

The initial values of the lateral and shear interaction soil springs were evaluated as follows. The lateral load-displacement relationship of n-piles is obtained using Green's functions by ring loads in a layered stratum (Kausel *et al.*, 1982).

$$\{u\} = [K_{PP}] \{P\} \tag{1}$$

where $\{u\}$ and $\{P\}$ are the vectors of lateral displacements and loads at m-nodes of each pile. $[K_{PP}]$ is an mn×mn interaction soil stiffness matrix of a pile group. Assuming that the displacement of each pile is identical at the same depth, $[K_{PP}]$ can be reduced to an m×m matrix $[K_P]$. Considering the displacement modes shown in Fig.

4, $[K_P]$ is decomposed to the lateral soil springs $[K_{a0}]$ and the shear soil springs $[K_{b0}]$ (Miyamoto *et al.*, 1995).

$$\{F\} = [K_P]\{U\} = \{[K_{a0}] + [K_{b0}]\}\{U\} \tag{2}$$

where

$$[K_{a0}] = \begin{bmatrix} K_{a0}^1 & & & \\ & K_{a0}^2 & & \\ & & K_{a0}^i & \\ & & & K_{a0}^m \end{bmatrix}, \quad [K_{b0}] = \begin{bmatrix} \square & & & \\ & \square & & \\ & & \square & \\ & & & \square \end{bmatrix}, \quad \square = K_{b0}^i \begin{bmatrix} 1 & -1 \\ -1 & 1 \end{bmatrix}$$

The initial lateral and shear soil springs were calculated at low frequency (f=0.1Hz) using degraded shear moduli and damping factors corresponding to the effective shear strain ($0.65\gamma_{max}$) of each layer. The effective shear strain was also obtained using DESRA in the condition that considered the nonlinear shear stress-strain relationship only, and not the changes in effective stress. The nonlinearity of the soil springs were assumed as shown in Fig. 5. The lateral load-displacement relationship was idealized by the Hardin-Drnevich model with

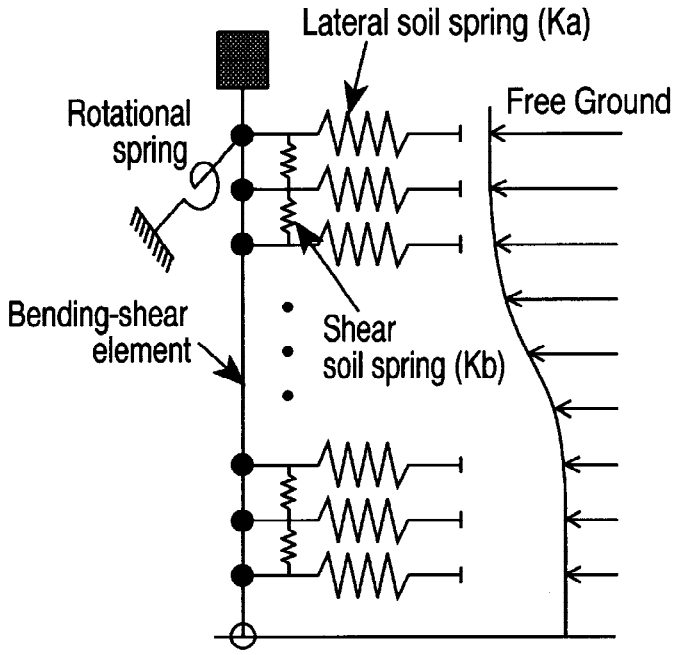

Fig. 3 Numerical model of soil-pile foundation system for correlation analysis

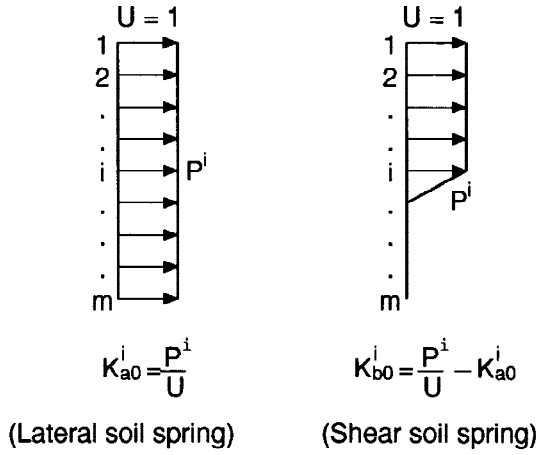

Fig. 4 Displacement modes for evaluating the lateral and shear soil springs

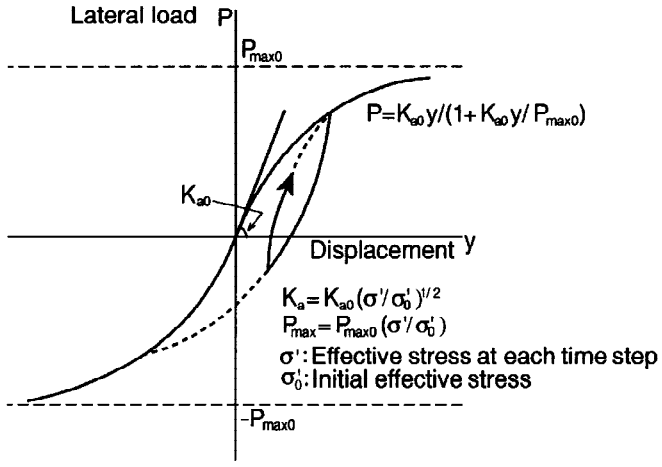

Fig. 5 Nonlinear lateral load-displacement relationship of the lateral soil spring

the Masing rule. The initial ultimate lateral soil resistance P_{max0} at each depth was evaluated after Broms(1965).

$$P_{max0} = 3\,\sigma_0'\,k_p\,d\,l\,n \tag{3}$$

where $k_p=(1+\sin\phi')/(1-\sin\phi')$, ϕ' is internal friction angle of the sand, d is pile diameter, l is pile length equivalent to the i-th node and n is the number of piles. The soil springs and the ultimate lateral soil resistances were also modified in accordance with the generation and dissipation of excess pore water pressures at each depth.

The physical properties of Toyoura sand are summarized in Table 1. In the centrifuge model tests, the permeability kv is increased 45 times corresponding to the similarity rule. The initial shear moduli G_0 was estimated from

$$G_0 = A\,\frac{(2.17-e)^2}{(1+e)}(\sigma_{m0}')^{1/2} \tag{4}$$

where e is void ratio and σ_{m0}' is initial mean effective stress. The coefficient A was modified to coincide with the resonant frequency of the free soil deposit in Test-A1, the low input case. Fig. 6 presents the liquefaction resistance curve compared with test results for Toyoura sand.

Table 1 Physical properties of Toyoura sand

Specific Gravity	Gs	: 2.64
Maximum Void Ratio	e_{max}	: 0.977
Minimum Void Ratio	e_{min}	: 0.605
Permeability (m/sec)	kv	: 1.62×10^{-4}
Relative Density	Dr	: 60%
Internal friction angle	ϕ'	: 36.6°
Coeff. of earth pressure at rest	K_0	: 0.4
Initial Shear Modulus (tf/m^2)	G_0	:970~6020
Parameters of DESRA		
C1=1.0, C2=0.4, C3'=0.161, C4=0.5,		
k2=0.0125~0.0195tf/m^2, m=0.43, n=0.62		

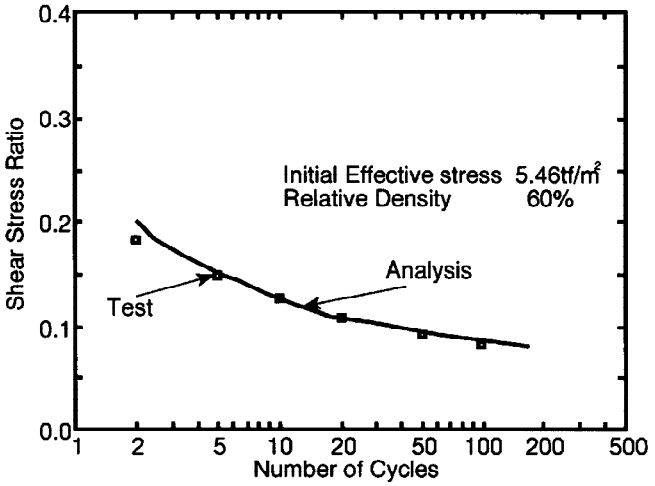

Fig. 6 Comparisons of the calculated liquefaction resistance curve with test results

4 TEST RESULTS AND CORRELATION ANALYSES

The results shown below are indicated in prototype scale. Fig. 7 compares the maximum excess pore water pressures in the surrounding soil (PP2, PP4, PP6) for Test-A1 and Test-A2 with the initial effective stress. For Test-A1, the pore water pressure didn't increase and the nonlinearity of the soil can be considered to be weak. Thus, the study for Test-A1 was conducted by the linear analysis. For Test-A2, the upper 3m of the soil was completely liquefied and the analytical results coincide well with the test results. There was little difference between the pore water pressure recorded in the middle of the pile group (PP1, PP3, PP5) and that recorded in the surrounding soil at each corresponding depth. It seems that the existence of the pile group doesn't have much effect on the generation of the excess pore water pressure. The soil responses and pore water pressure generation for Test-B1 and Test-B2 were almost the same as those for Test-A1 and Test-A2, respectively. Test-B1 was also studied by the linear analysis.

Fig. 8 compares the time histories of the accelerations and the pile bending moment for Test-A1. The maximum acceleration responses in the soil (GL-0.5m, AH10) and on the structure (AH11) occurred at about 2 seconds, corresponding to the input acceleration (AH1). The wave form of the pile bending moment at GL-0.0m (SG9) was similar to the acceleration on the structure (AH11). This implies that the pile bending moment near the pile head is predominantly induced by the inertial force of the structure.

The time histories of the accelerations, the pile bending moments and excess pore water pressure ratio for Test-A2 are shown in Fig. 9. The pore water pressure at GL-3.6m (PP6) began to increase around 2 seconds and leveled off around 5 seconds. Due to the occurrence of liquefaction, the high frequency components of the acceleration decreased at GL-0.5m in the soil (AH10) compared with those of Test-A1. The response acceleration

on the structure (AH11) also contained few high frequency components and large responses were seen from 2-5 and 11-12 seconds. The pile bending moment at GL-0.0m (SG9) resembled the acceleration response of the structure in shape and became large in the same periods. The one at GL-14.4m, however, contained relatively high frequency components and was rather similar to the input acceleration (AH1). It can be considered that the pile bending moment in the deeper part of the soil was largely influenced by the response of the soil deposit. The analyses predict fairly well the test results, including the variation with time of excess pore water pressure and the pile bending moments at various depths.

Fig.10 shows the Fourier spectra ratios on the structure (AH11) to the input acceleration (AH1) for Test-A1 and Test-A2. Table 2 summarizes the maximum accelerations on the structure (AH11) and the amplification ratios of the maximum accelerations on the structure to the input acceleration (AH1). For Test-A1, the first peak of the Fourier spectra ratios represents the first mode of the soil deposit. The second one corresponds to both the second mode of the soil deposit and the first mode of the soil-pile foundation system. The maximum acceleration was amplified to about 4 times that of the input acceleration for Test-A1 and to almost the same for Test-B1. For Test-A2, the amplitude of the Fourier spectra ratio was significantly reduced, especially in the high frequency range, due to the occurrence of liquefaction. The amplitude of the first peak decreased and the second one was not clear because of the decrease in rigidity and the increase in

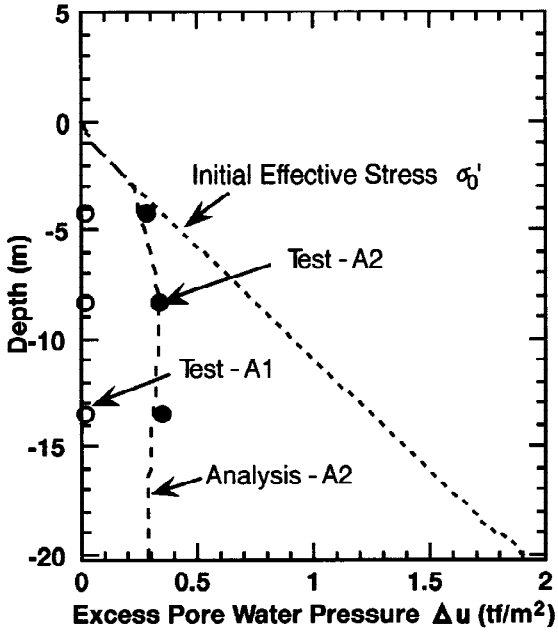

Fig. 7 Comparisons of the calculated excess pore water pressure for Test-A1 and Test-A2

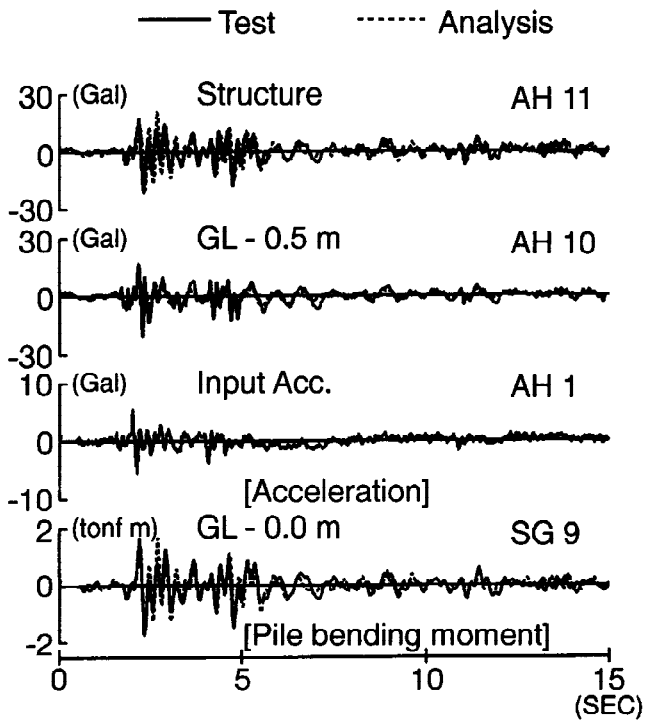

Fig. 8 Comparisons of the calculated time histories for Test-A1

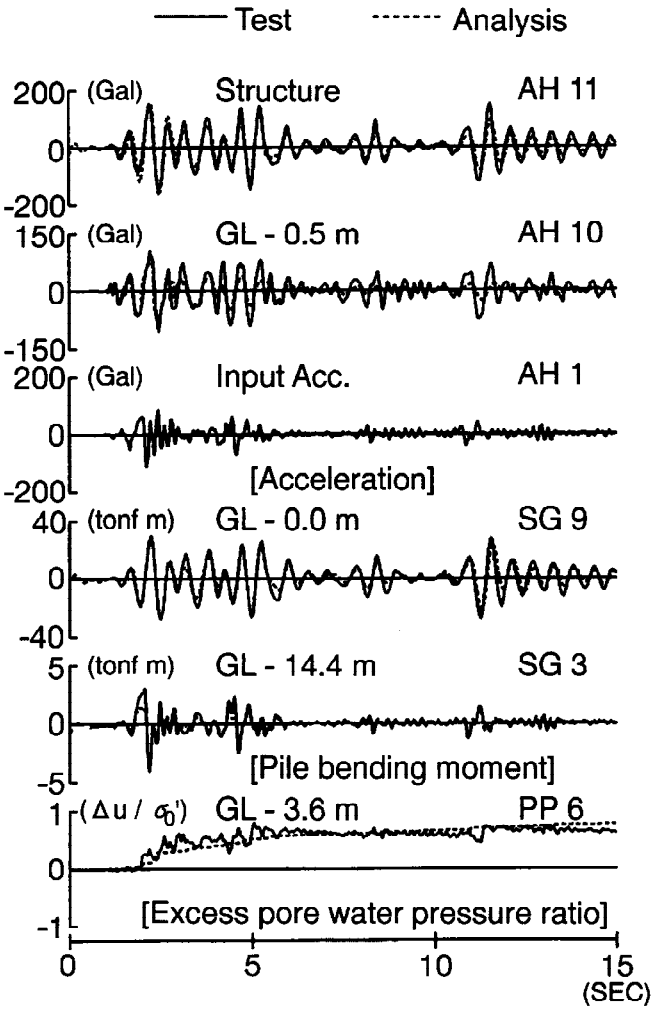

Fig. 9 Comparisons of the calculated time histories for Test-A2

damping of the soil. The amplification ratios for Test-A2 and Test-B2 were small compared with those for Test-A1 and Test-B1. This means the inertial force of the structure decreased when liquefaction occurred. The analytical results well express the differences between the Fourier spectra ratios of Test-A1 and Test-A2 and good predictions were obtained for the maximum accelerations of the structures.

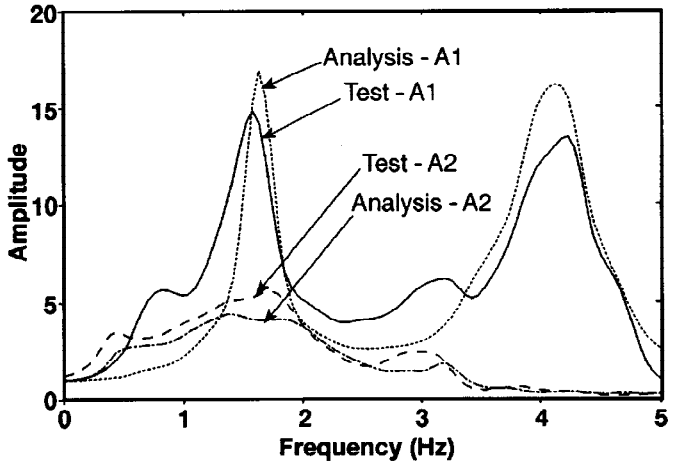

Fig.10 Comparisons of Fourier spectra ratios on the structure (AH11) to the input acceleration (AH1)

Table 2 Comparisons of maximum accelerations on the structure and amplification ratios of maximum accelerations on the structure to the input accelerations

		Test	Analysis
A 1	Amax (Gal) (AH11)	21.1	21.3
	Ratio (AH11/AH1)	3.6	3.6
A 2	Amax (Gal) (AH11)	149.4	166.4
	Ratio (AH11/AH1)	1.3	1.5
B 1	Amax (Gal) (AH11)	14.6	11.2
	Ratio (AH11/AH1)	4.7	3.6
B 2	Amax (Gal) (AH11)	160.7	120.5
	Ratio (AH11/AH1)	1.5	1.1

5 STUDY ON PILE BENDING MOMENT

The distributions of maximum pile bending moments were compared to study the effect of the weight of the structure and the level of the input acceleration on them.

Fig. 11 plots the distributions of the maximum bending moments of the pile normalized by the maximum input accelerations. The left part of the figure compares the differences in the input accelerations using the results for Test-A1 and Test-A2. The maximum bending moments occurred at the pile head in both cases. A remarkable change, however, was seen in the distributions of the maximum bending moments for Test-A1 and Test-A2. The bending moment for Test-A2 was smaller near the pile head, although it became large around GL-5m. The bending moment for Test-A2 was larger in the part of the pile deeper than GL-10m. These tendencies are well expressed by the analyses. The right part of the figure compares the differences in the weights of the structures using the results for Test-A2 and Test-B2. There was a big difference between the pile bending moments of Test-A2 and Test-B2 around the pile head and no swelling was seen around GL-5m for Test-B2. Under GL-12m they were almost the same. This indicates that the inertial force didn't have much affect on pile bending moment in the deep part of the pile. The analytical results are in good agreement with the test results except near the pile tip, because the behavior at the pile tip was considered to be slightly different from the idealized pin condition in the tests.

To study the influence of the inertial force and displacement of the soil deposit on pile bending moments, the moment induced by the inertial force, hereafter called "inertial" component, and the one caused by the soil displacement, hereafter called "kinematic" component, were calculated independently. The kinematic components were evaluated by means of the same analytical procedure using a pile-foundation model with a massless structure. The inertial components were obtained by subtracting the kinematic components from the total bending moments in the time domain. It is necessary to bear in mind that this procedure is not rigorous because the soil was not in a linear elastic condition for Test-A2 and Test-B2.

Fig.12 shows the results for Test-A1 and Test-A2 with a heavy structure and Fig.13 shows the results for Test-B1 and Test-B2 with a relatively light structure. Each figure is normalized by the maximum input accelerations. For Test-A1, the inertial component extended from the pile head to GL-10m and comprised almost the total moment till GL-7m. The kinematic component extended from the pile tip to the pile head and determined the total moment under GL-7m. For Test-A2, the inertial component was smaller than for Test-A1 near the pile head and the contribution of the kinematic component became large. These are because the inertial force of the

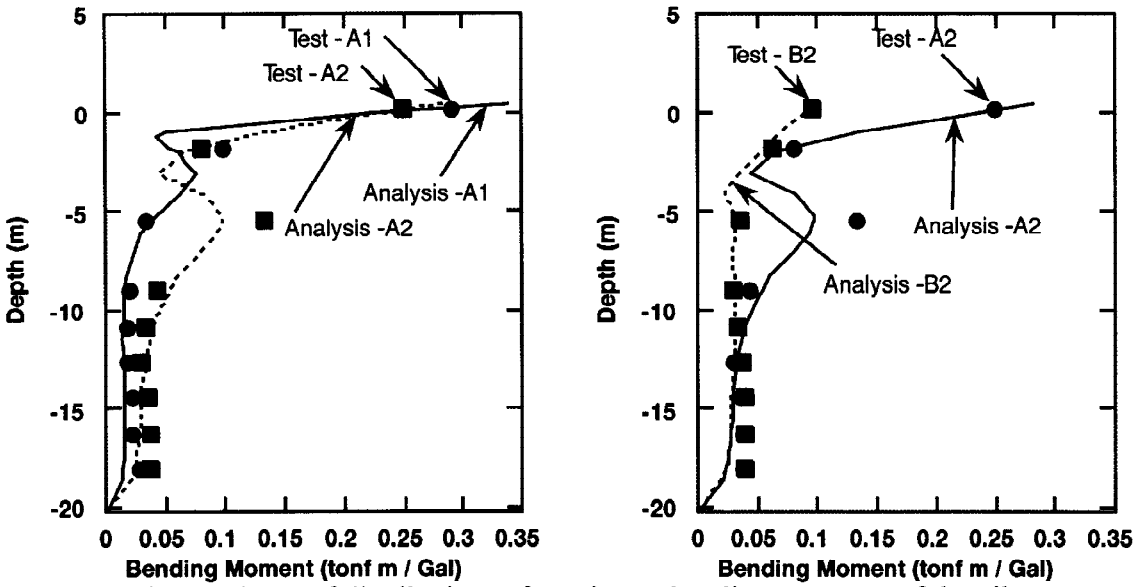

Fig.11 Comparisons of distributions of maximum bending moments of the pile (The pile bending moments are normalized by the maximum input accelerations.)

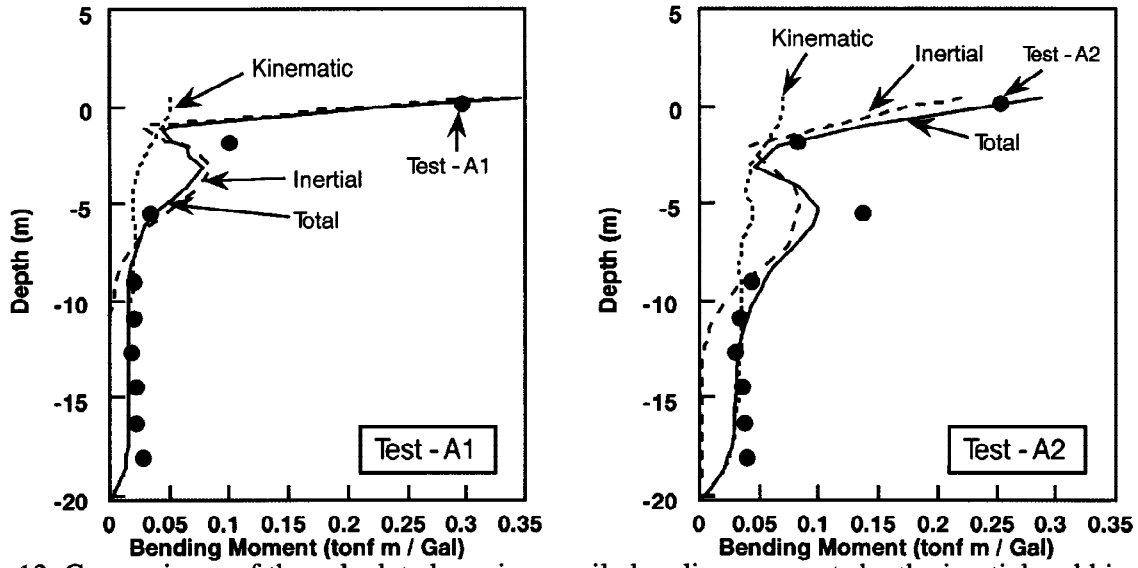

Fig. 12 Comparisons of the calculated maximum pile bending moments by the inertial and kinematic interactions for Test-A1 and Test-A2 (The pile bending moments are normalized by the maximum input accelerations.)

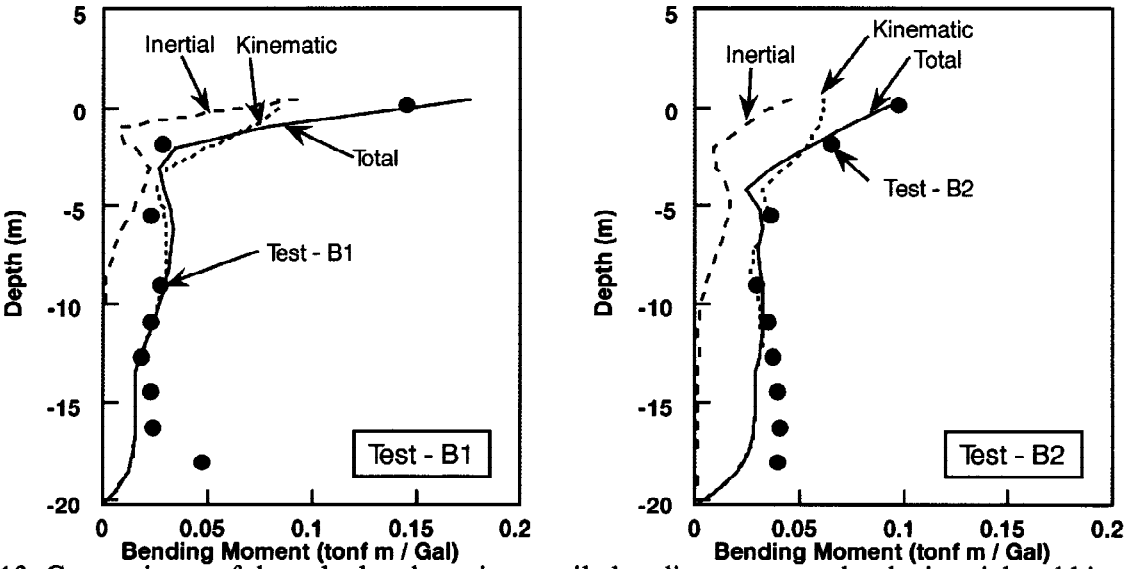

Fig.13 Comparisons of the calculated maximum pile bending moments by the inertial and kinematic interactions for Test-B1 and Test-B2 (The pile bending moments are normalized by the maximum input accelerations.)

structure to the input acceleration decreased for Test-A2 as shown in Table 2, and the relative displacement of the soil increased due to liquefaction. Since the soil rigidity decreased due to the excess pore water pressure generation and soil nonlinearity, the inertial component extended deeper than Test-A1 and caused the large pile bending moment around GL-5m. It can be seen that for Test-A2 the increase in pile bending moments under GL-10m was caused by the increase in the kinematic component due to the excess pore water pressure generation and the soil nonlinearity. For Test-B1, the inertial component was small compared with that of Test-A1 and its contribution was limited to GL-8m. The kinematic component was equivalent to the inertial component at the pile head but governed the pile bending moments in most parts. For Test-B2, the kinematic component was larger than the inertial component from the pile head to the pile tip due to the small inertial force and the large relative displacement of the soil. Compared with Test-A2, it should be pointed out that the significant reduction in pile bending moments around pile head was caused by the decrease in the inertial component.

6 CONCLUSIONS

The concluding remarks of this study are as follows:

1. Shaking table tests for a pile foundation model were performed under a centrifuge acceleration of 45g. Due to liquefaction, a significant reduction can be seen in the amplification ratio of response acceleration of the pile foundation to the input acceleration. High frequency components of the response acceleration decrease with the soil nonlinearity and the excess pore water pressure generation.
2. The numerical model of the soil-pile foundation system which consists of beam elements and nonlinear interaction springs follows well the pile-foundation response in a liquefiable sand deposit.
3. The pile bending moments near the pile head are greatly affected by the inertial force of the structure. With increase in input acceleration, the effect of the inertial force on the pile bending moment becomes smaller corresponding to the decrease in response acceleration of the structure but reaches a deeper part of the pile due to the decrease in soil rigidity.
4. The pile bending moments caused by the displacement of the soil deposit contribute from pile tip to pile head and are predominant in the deeper part of the pile. With increase in input acceleration, they become larger and their contribution to the total pile bending moment increases.

REFERENCES

Broms B. B. (1965) Design of laterally loaded piles. *Journal of the Soil Mechanics and Foundation Division, ASCE*, **91**, 79-99

Finn W.D.L., Lee K.W., and Martin G.R. (1977) An effective stress model for liquefaction. *Journal of the Geotechnical Eng. Division, ASCE*, **103**, 517-533

Kausel E. and Peek R. (1982) Dynamic loads in the interior of a layered stratum -An explicit solution. *Bulletin of the Seismological Society of America*, **72**, 1459-1481

Miyamoto, Y., Sako Y., Miura K., Scott R. F. and Hushmand B. (1992). Dynamic behavior of pile group in liquefied sand deposit. *Proc. of 10WCEE*, **3** ,1749-1754

Miyamoto, Y., Sako Y., Kitamura E. and Miura K. (1995). Earthquake response of pile foundation in nonlinear liquefiable soil deposit. *J. Struct. Constr. Eng., AIJ*, **471** ,41-50